JOURNAL OF SPACECRAFT AND ROCKETS
Vol. 30, No. 1, January–February 1993

Navier-Stokes Solutions with Surface Catalysis for Martian Atmospheric Entry

Y.-K. Chen*
Eloret Institute, Palo Alto, California 94303
W. D. Henline† and D. A. Stewart†
NASA Ames Research Center, Moffett Field, California 94035
and
G. V. Candler‡
North Carolina State University, Raleigh, North Carolina 27612

In this study numerical solutions have been obtained for axisymmetric hypersonic nonequilibrium CO_2 flow over a large-angle blunt cone with appropriate surface boundary conditions to account for energy and mass conservation at the body surface. The flowfield is described by the Navier-Stokes equations and multicomponent conservation laws that account for both translational and internal vibrational nonequilibrium effects. Complete forebody solutions have been obtained for the peak heating point of the Mars entry trajectory specified in the proposed NASA MESUR (Mars Environmental Survey) project. In these solutions, radiative equilibrium wall temperature and surface heating distributions are determined over the MESUR aeroshell forebody with varying degrees of surface catalysis. The aeroshell nose radius is 0.425 m, and freestream conditions occur at an altitude of 41,668 m, ambient density of 0.2687×10^{-3} kg/m^3, and velocity of 6155 m/s. The effects of gas kinetics, surface catalysis, and transport properties on the surface heating are examined. The results identify some important issues in the prediction of surface heating for flows in thermochemical nonequilibrium and show that the Navier-Stokes code used herein provides useful information for thermal protection system design and materials selection.

Nomenclature

C_i = species i mass fraction
C_P = specific heat, J/kg-K
D = diffusion coefficient, m^2/s
e_v = vibrational energy, J/kg
H_t = total enthalpy, J/kg
h = enthalpy, J/kg
J_i = mass flux of species i, kg/m^2-s
k_i = surface catalysis reaction rate, m/s
k_T = conductivity for translational energy, W/m-K
k_v = conductivity for vibrational energy, W/m-K
L_e = Lewis number
M = molecular weight, kg/mole
M_f = freeze Mach number
P_r = Prandtl number
P_t = total impact pressure, N/m^2
q_w = surface heat flux, W/m^2
R = gas constant, kg-m^2/mole-K-s^2
R_b = vehicle base radius, m
R_c = vehicle corner radius, m
R_e = Reynolds number
R_n = vehicle nose radius, m
T_t = translational temperature, K
T_v = vibrational temperature, K
T_w = surface temperature, K
u = velocity, m/s^2
γ = surface reaction rate coefficient
ϵ = surface total hemispherical emittance
η = coordinate normal to surface, m
μ = viscosity, kg/m-s
ρ = density, kg/m^3
σ = Stefan-Boltzmann constant, W/m^2-K^4
ω = relaxation factor

Received May 22, 1992; revision received Aug. 26, 1992; accepted for publication Aug. 27, 1992. This paper is declared a work of the U.S. Government and is not subject to copyright protection in the United States.

*Research Scientist; currently, on-site contractor, NASA Ames Research Center.
†Research Scientist, Thermal Protection Materials Branch.
‡Assistant Professor, Mechanical Engineering Department.

Introduction

DURING a Martian entry, the CO_2-N_2 gas mixture in the shock layer that envelops a vehicle forebody heatshield is at high temperature and can be out of thermochemical equilibrium. The degree of displacement from equilibrium can have a significant effect on the heat transfer rate to the forebody heatshield. The gas chemistry in the shock layer and the temperature and species concentration gradients near the surface are dependent on the position of the bow shock wave relative to the forebody. Thus, the analysis for a nonequilibrium flow must include appropriate transport models and surface boundary conditions to accurately predict the heating rate distribution over a vehicle traveling at hypersonic speed.

There have been previous studies of this problem using techniques similar to those discussed here. An inviscid shock layer calculation by an inverse method with finite rate chemistry was done by Evans et al.[1] to investigate the effect of nonequilibrium ablation chemistry on Viking radio blackout. Also, Candler[2] solved the two-dimensional axisymmetric Navier-Stokes equations with a multicomponent and multiple temperature model to describe the behavior of an aerobrake passing through the Martian atmosphere. In that calculation, the surface was assumed to be isothermal and noncatalytic. The gas kinetics examined in those two previous studies were mostly derived from the work of McKenzie.[3] More recently, an extensive study of the gas kinetics for the Martian atmosphere was done by Park et al.[4] In addition, Stewart et al.[5,6] demonstrated that surface catalysis can play an essential role on the nonablating surface heating for air flows. Subsequently, Chen[7] has predicted the surface heating over the Mars Environmental Survey (MESUR) project's aeroshell using the codes AMIR,[8] BLIMPK,[9] and VSL[10] with surface catalysis in

a CO_2 atmosphere. This most recent study has found that, for a noncatalytic surface, McKenzie's[3] kinetics predicted much higher surface heating than those of Park et al.[4] and that, for a fully catalytic surface, the surface heating was relatively insensitive to the gas kinetics.

The purpose of the present study is to predict the surface heating over a high-angle blunt cone (typified by the MESUR probe geometry with entry velocity equal to 7 km/s) using a Navier-Stokes code (adapted from Candler[2]) with appropriate boundary conditions to conserve energy and mass at the wall. The nose radius of the MESUR probe is 0.425 m, and computations were performed at near peak heating condition at an altitude of 41,668 m, ambient density of 0.2687×10^{-3} kg/m^3, and velocity of 6155 m/s. The gas kinetics developed by Park et al.[4] and McKenzie,[3] respectively, are implemented into the code, and a first-order surface catalysis model for CO_2-N_2 mixtures is also included. Numerical problems typically encountered near the stagnation point have been minimized in the solutions obtained. Final solutions are obtained through local and global iterations and are compared with those of the viscous shock layer (VSL) code and data taken from a NASA Ames 1.07-m (42-in.) shock tunnel experiment. Since at this point knowledge of the physicochemical nature of high temperature CO_2-N_2 systems is in its infancy, the uncertainties associated with variations in gas kinetics, surface catalysis, and transport properties on surface heating are examined.

Governing Equations

The governing equations used here to describe the flow over a hypersonic vehicle were developed by Lee.[11] Because of the voluminous nature of these equations, the details of their formulation will not be presented in this paper. However, they may be characterized as representing a flowfield in thermochemical nonequilibrium. Determination of the dynamics of the flow requires the solution of species mass conservation equations, a mass-averaged momentum equation, a vibrational energy equation, the total energy equation, and the equation of state. An eight-species (N_2, O_2, NO, O, N, C, CO, and CO_2) gas model is considered. Based on the formulation developed by Tauber and Sutton[12] and Park et al.[4] and the solutions presented in Ref. 7, we conclude that the effects of ionization and radiation on the surface heating are not important for the cases examined in this study. Additionally, ablation and phase change at the surface are ignored in the calculations.

We assume that the rotational energy modes are in equilibrium with the translational modes and that there is a unique vibrational temperature at each point in the flowfield. The total vibrational energy of the CO_2-N_2 mixture is the sum of the individual vibrational energies of each species. A simple harmonic oscillator model is used to describe the vibrational potential of each vibrational mode of the molecules. CO_2 has three vibrational modes, one of which is doubly degenerate. The rate at which these vibrational energies relax toward the translational energy is assumed to behave according to the Landau-Teller relaxation expression.[13] The vibrational relaxation time is determined from an expression due to Millikan and White.[14] The vibrational energy constants used in this expression are listed in Ref. 2.

Gas Kinetics

The chemical reactions between the eight species considered in this work are taken to be

$$CO_2 + M_1 = CO + O + M_1 \tag{1}$$

$$CO + M_2 = C + O + M_2 \tag{2}$$

$$N_2 + M_3 = 2N + M_3 \tag{3}$$

$$O_2 + M_4 = 2O + M_4 \tag{4}$$

$$NO + M_5 = N + O + M_5 \tag{5}$$

$$CO + N = NO + C \tag{6}$$

$$CO + CO = CO_2 + C \tag{7}$$

$$CO + O = O_2 + C \tag{8}$$

$$N_2 + O = NO + N \tag{9}$$

$$NO + CO = CO_2 + N \tag{10}$$

$$NO + O = O_2 + N \tag{11}$$

$$CO_2 + O = O_2 + CO \tag{12}$$

where the various M represent any species that acts as a collision partner (i.e., a third body). Each reaction is governed by forward and backward reaction rate coefficients k_f and k_b, which are of the form

$$k_f = C_f T^{Df} \exp(-E_f \times 1000/T) \tag{13}$$

$$k_b = C_b T^{Db} \exp(-E_b \times 1000/T) \tag{14}$$

where C_f, C_b, D_f, D_b, E_f, and E_b are constants. Two sets of gas kinetics are studied in this work; one is from Park et al.,[4] and the other is from McKenzie.[3] The forward and backward reaction rates and the third-body reaction rates for these two models are listed in Table 1. The backward reaction rates of Park et al. are derived from the equilibrium constants calculated based on ratios of the McKenzie reaction rates. It is assumed that the forward dissociation reactions (the first five reactions) are governed by the geometric average of the translational and vibrational temperatures; that is, $T = \sqrt{(T_t T_v)}$. This is the $T_t T_v$ model of Park[15] originally developed for reacting air. However, the theoretical basis for the use of this governing temperature is similar for reacting CO_2 (Ref. 2). The recombination rates depend only on the translational temperature of the impacting particles. The other seven reactions are assumed also to be governed only by the translational temperature. These reactions are fundamentally different from the dissociation reactions. They involve a simple exchange of one atom for another on a molecule.

Surface Kinetics

In a CO_2-N_2 mixture, the following surface reactions are taken to be:

$$2N \rightarrow N_2 \tag{15}$$

$$2O \rightarrow O_2 \tag{16}$$

$$N + O \rightarrow NO \tag{17}$$

$$C + O \rightarrow CO \tag{18}$$

$$CO + O \rightarrow CO_2 \tag{19}$$

In this study, all of the reactions are assumed to be irreversible and first order, and the rate coefficient is expressed as follows for the ith reaction,

$$k_i = \gamma_i \sqrt{RT_w/2\pi M_i}; \qquad i = 1, 2, \ldots, 5 \tag{20}$$

with

Reaction 1:

$$J_N^1 = -k_1 \rho_N, \qquad J_{N_2}^1 = k_1 \rho_N \tag{21a}$$

Reaction 2:

$$J^2_O = -k_2\rho_O, \qquad J^2_{O_2} = -k_2\rho_O \tag{21b}$$

Reaction 3:

$$J^3_O = -k_3\sqrt{\rho_N\rho_O}, \qquad J^3_N = -k_3(M_N/M_O)\sqrt{\rho_N\rho_O}$$
$$J^3_{NO} = k_3\sqrt{\rho_N\rho_O} \tag{21c}$$

Reaction 4:

$$J^4_O = -k_4\sqrt{\rho_C\rho_O}, \qquad J^4_C = -k_4(M_C/M_O)\sqrt{\rho_C\rho_O}$$
$$J^4_{CO} = k_4(M_{CO}/M_O)\sqrt{\rho_C\rho_O} \tag{21d}$$

Table 1 Forward and backward reaction rates and third-body reaction rates for models of Park et al.[4] and McKenzie[3]

Equation number	C_f	D_f	E_f	C_b	D_b	E_b
	Reaction rate coefficients cm^3-mole^{-1}-s^{-1} or cm^6-mole^{-2}-s^{-1}					
			Park et al.			
(1)	3.70×10^{14}	52.5	0.0	6.10×10^9	−10.24	0.75
(2)	2.30×10^{19}	129.0	−1.0	5.13×10^{17}	0	−1.0
(3)	7.00×10^{21}	113.2	−1.6	4.27×10^{20}	0	−1.6
(4)	2.00×10^{21}	59.5	−1.5	2.00×10^{18}	0	−1.0
(5)	5.00×10^{15}	75.5	0.0	4.27×10^{15}	0	0.0
(6)	2.86×10^{11}	53.63	0.5	2.60×10^{10}	0	0.5
(7)	2.33×10^9	65.71	0.5	4.60×10^{12}	0	−0.25
(8)	3.90×10^{13}	69.2	−0.18	1.34×10^{14}	0	−0.43
(9)	6.40×10^{17}	38.3	−1.0	1.39×10^{17}	0	−1.0
(10)	4.59×10^8	12.07	0.5	9.90×10^{13}	0	−0.25
(11)	8.40×10^{12}	19.45	0.0	2.68×10^{11}	0	0.5
(12)	1.70×10^{13}	26.5	0.0	3.33×10^{10}	22.5	0.5
			McKenzie			
(1)	1.20×10^{11}	34.34	0.5	2.00×10^6	−28.4	1.25
(2)	4.48×10^{19}	128.9	−1.0	1.00×10^{18}	0	−1.0
(3)	2.46×10^{19}	113.2	−1.0	1.50×10^{18}	0	−1.0
(4)	9.05×10^{18}	59.37	−1.0	9.00×10^{15}	0	−0.5
(5)	4.09×10^{18}	75.33	−1.0	3.50×10^{18}	0	−1.0
(6)	2.86×10^{11}	53.6	0.5	2.60×10^{10}	0	0.5
(7)	2.33×10^9	65.71	0.5	4.60×10^{12}	0	−0.25
(8)	2.73×10^{12}	69.54	0.5	9.40×10^{12}	0	0.25
(9)	7.35×10^{11}	37.94	0.5	1.60×10^{11}	0	0.5
(10)	4.59×10^8	12.07	0.5	9.90×10^{12}	0	−0.25
(11)	2.98×10^{11}	19.46	0.5	9.50×10^9	0	1.0
(12)	2.54×10^{11}	27.69	0.5	5.00×10^8	23.9	1.0

Multipliers for third-body reactions

	M_1	M_2	M_3	M_4	M_5
			Park et al.		
CO_2	1.0	1.0	1.0	1.0	22.0
CO	1.0	1.95	1.0	1.0	1.0
N_2	1.0	1.0	1.0	1.0	1.0
O_2	1.0	1.0	1.0	1.0	1.0
NO	1.0	1.0	1.0	1.0	22.0
C	1.0	14.8	4.28	5.0	22.0
N	1.0	14.8	0.0	5.0	22.0
O	1.0	14.8	4.28	5.0	22.0
			McKenzie		
CO_2	1.0	1.0	1.0	1.0	1.0
CO	1.0	1.0	1.0	1.0	1.0
N_2	1.0	1.0	1.0	1.0	1.0
O_2	1.0	1.0	1.0	1.0	1.0
NO	1.0	1.0	1.0	1.0	1.0
C	1.0	1.0	1.0	1.0	1.0
N	1.0	1.0	1.0	1.0	1.0
O	1.0	1.0	1.0	1.0	1.0

Reaction 5:

$$J^5_O = -k_5\sqrt{\rho_{CO}\rho_O}, \qquad J^5_{CO} = -k_5(M_{CO}/M_O)\sqrt{\rho_{CO}\rho_O}$$
$$J^5_{CO_2} = k_5(M_{CO_2}/M_O)\sqrt{\rho_{CO}\rho_O} \tag{21e}$$

where γ_i is the recombination rate coefficient, which may, in general, be a function of wall temperature and pressure. For air, attempts have been made to correlate recombination rate coefficients and wall temperature, such as the reaction cured glass (RCG) kinetics of Kolodziej and Stewart.[16] However, for the CO_2-N_2 mixture, no such study has been conducted. The species concentrations of C and N near the surface are extremely low.[7] Given this, the effects of N + N, N + O, and C + O surface reactions on the surface heating and flow structure are negligibly small. Therefore, in this study only reactions 2 and 5 (O + O and CO + O recombinations) are considered, and reactions 1, 3, and 4 are ignored.

Transport Properties

The viscosity and thermal conductivity of the gas mixtures encountered here are calculated using Wilke's semiempirical mixing rule.[17] The thermal conductivity for translational and vibrational energy of each species is derived from the Eucken relation.[13] The model for viscosity of each species was developed by Blottner et al.,[18] and the constants for the curve fits are found in Refs. 2 and 18. The diffusive mass fluxes of each species are assumed to obey Fick's Law of isotropic diffusion. The species diffusion coefficients are taken from Lee[11] and are derived by assuming a constant Schmidt number of 0.5. Similarly, the thermal conductivity of translational energy can also be calculated by assuming a constant Prandtl number with $k_T = C_P\mu/P_r$; the species binary diffusion coefficient can also be evaluated based on an assumed Lewis number with $D = L_e k_T/C_P\rho$.

Surface Boundary Conditions

A no-slip velocity condition and zero normal pressure gradient are imposed at the wall. This is under the assumptions of continuum flow. The surface is assumed to be at radiative equilibrium. If the conduction loss through the wall, radiation from the flow to the wall, ablation, and phase change are negligible, then the surface energy balance equation becomes

$$q^n_w = \left(k_t\frac{\partial T_t}{\partial\eta} + \sum_{j=1}^{N_v} k_{v_j}\frac{\partial e_{v_j}}{\partial\eta} + \sum_i h_i\rho D_i\frac{\partial C_i}{\partial\eta}\right)^n_w = \epsilon\sigma(T^n_w)^4 \tag{22}$$

and

$$T^n_v = T^n_t = T^n_w \tag{23}$$

Under the same assumptions, the species conservation equations are

$$\sum_{r=1}^{N_r} J^r_i = -\rho D_i\frac{\partial C_i}{\partial\eta}\Big|_w \tag{24}$$

where J is defined in Eqs. (21); $i = CO_2$, CO, N_2, O_2, NO, C, N, and O; N_v is the total number of vibrational energies; and N_r is the total number of surface reactions. In each global iteration, the wall temperature is updated based on the energy balance and is expressed as

$$T^{n+1}_w = \left[\left(\frac{q_w}{\epsilon\sigma}\right)^{1/4} - T^n_w\right]\omega + T^n_w \tag{25}$$

From Eqs. (21) and (24), the species concentrations at the wall are updated based on

$$C^{n+1}_{i,w} = (C^n_{i,w+1} - C^n_{i,w})\omega + C^n_{i,w}, \qquad i = C, N, N_2, NO \tag{26}$$

$$C_{O,w}^{n+1} = \left\{ \left[\frac{C_{O,w+1}^{n}}{(\Delta\eta k_2/D_O) + 1} + \frac{C_{O,w+1}^{n}}{(\Delta\eta k_5/D_O)(C_{CO,w}^{n}/C_{O,w}^{n})^{1/2} + 1} \right] - C_{O,w}^{n} \right\} \omega + C_{O,w}^{n} \quad (27)$$

$$C_{CO,w}^{n+1} = \left\{ \left[\frac{C_{CO,w+1}^{n}}{(M_{CO}/M_O)(\Delta\eta k_5/D_{CO})(C_O^n/C_{CO}^n)^{1/2} + 1} \right] - C_{CO,w}^{n} \right\} \omega + C_{CO,w}^{n} \quad (28)$$

$$C_{O_2,w}^{n+1} = \{ [C_{O_2,w+1}^{n} + (\Delta\eta k_2/D_{O_2}) C_{O,w}^{n+1}] - C_{O_2,w}^{n} \} \omega + C_{O_2,w}^{n} \quad (29)$$

$$C_{CO_2,w}^{n+1} = 1 - [C_C + C_N + C_{N_2} + C_{NO} + C_O + C_{O_2} + C_{CO}]_w^{n+1} \quad (30)$$

Where n refers to the nth global iteration, and ω ($0 \leq \omega \leq 1$) is the relaxation factor ($\omega = 0.5$ was used in all of the calculations presented in this paper).

Solution Technique

The governing equations are solved in a fully coupled manner using an implicit, flux-split, Gauss-Seidel line relaxation numerical technique that effectively captures the forebody bow shock wave. The procedure for doing this has been discussed by Candler,[19] MacCormack,[20] and Candler and MacCormack.[21] The temperature and species concentrations at the wall are updated according to the boundary conditions [Eqs. (25–30)] through a global iteration procedure recently installed in the present code. In the first global iteration, the surface temperature, the species concentrations, and the whole flow structure are initially guessed. The flow solutions with isothermal and noncatalytic surface are the most commonly used initial guess. The computation is completed when both local and global iterations have simultaneously converged.

Based on our experience, numerical problems can occur in the vicinity of the stagnation streamline.[22,23] They usually manifest themselves as erroneous pressure and temperature gradients in the stagnation region of the blunt cone. From the tests done for this code, it was found that this problem may be reduced by means of an appropriate grid adaptation. If the y coordinate of the grid along the surface near the stagnation region is chosen according to $y = Y\sqrt{(i/N)}$, the predicted pressure and temperature distributions near the stagnation point appear to be better than those using a uniformly spaced grid. Here Y is the total radial distance y from the stagnation point, N is the total number of grid points in this region, and $i = 1, 2, \ldots, N$. With this prescription, the cell volumes in this region are nearly constant. Further research should be conducted to study the effect of the computational grid on the flow solution near the stagnation streamline.

Results and Discussion

Computations performed here were accomplished on the Cray YMP8/864 at NASA Ames Research Center. The Martian flight condition examined in this study is typical of peak heating for the MESUR probe 7 km/s entry. The MESUR heatshield is a 70-deg half-angle sphere cone with a nose radius of 0.425 m, $R_n/R_b = 0.5$, and $R_c/R_n = 0.1$ (Fig. 1). A 72×60 grid is used in all of the calculations, and the minimum distance between grid points is $2 \times 10^{-4} R_n$. The minimum cell Reynolds number is about 0.2. In the direction along the surface, a constant volume grid is applied near the stagnation point region, and a uniformly spaced grid is applied elsewhere.

As a consistent check of the present code, a test calculation was performed using conditions similar to a shock tunnel experiment (in CO_2) using the same forebody shape as the

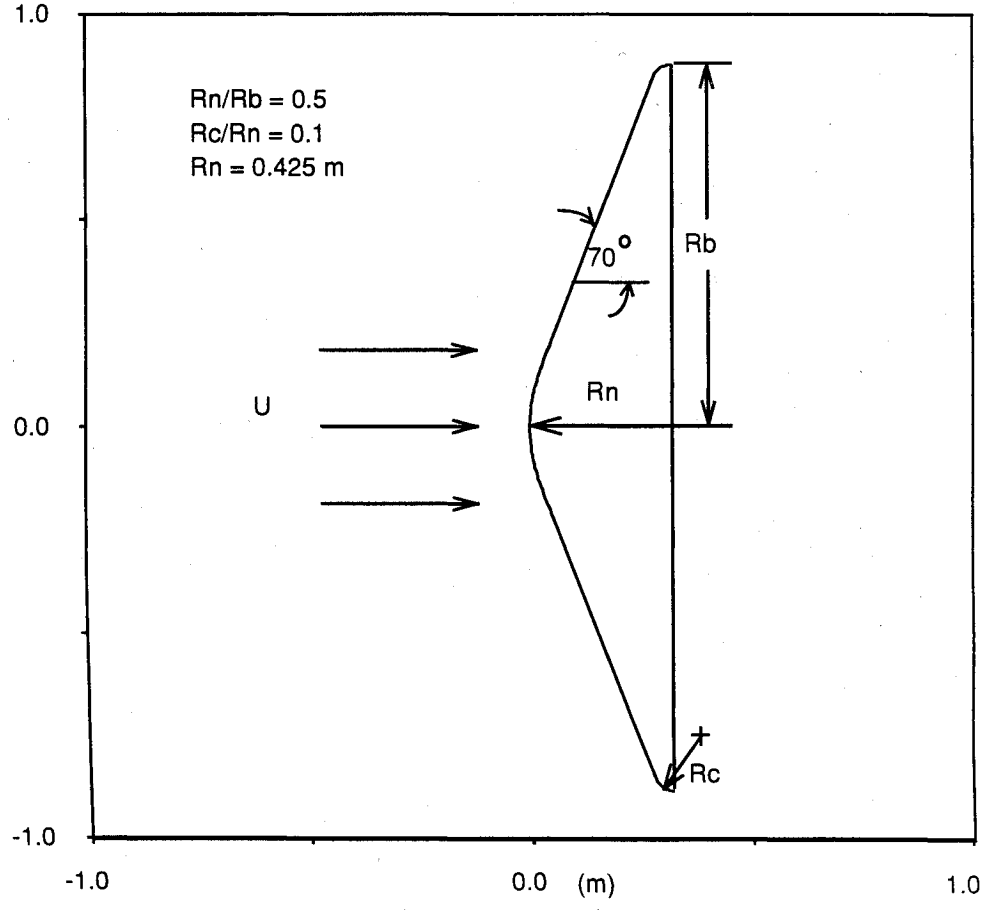

Fig. 1 MESUR aeroshell configuration.

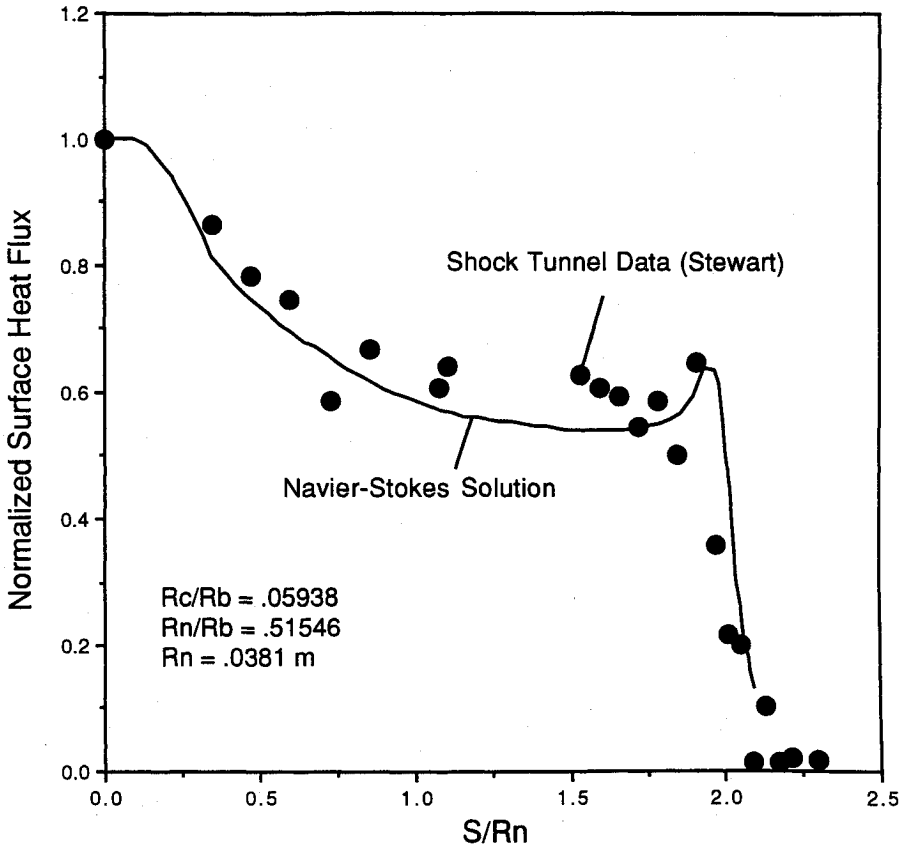

Fig. 2 Normalized surface heat flux distributions: H_t = 4.7 MJ/kg, P_t = 0.0516 atm, and M_f = 3.5.

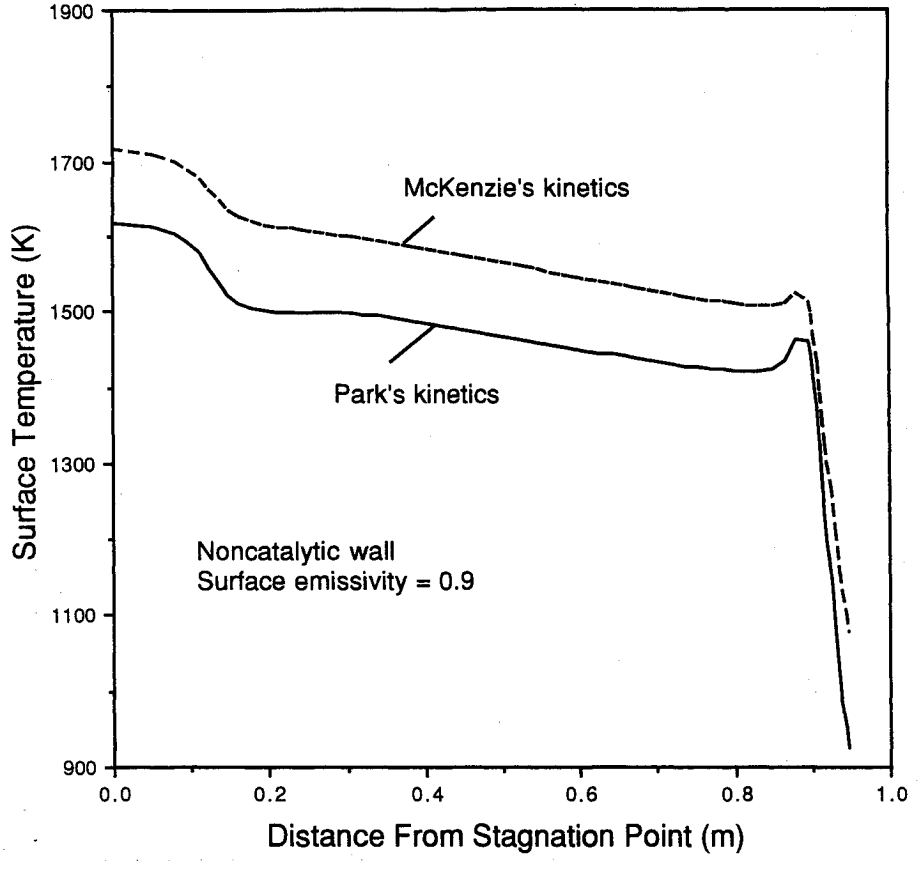

Fig. 3a Radiative equilibrium temperature profiles along surface.

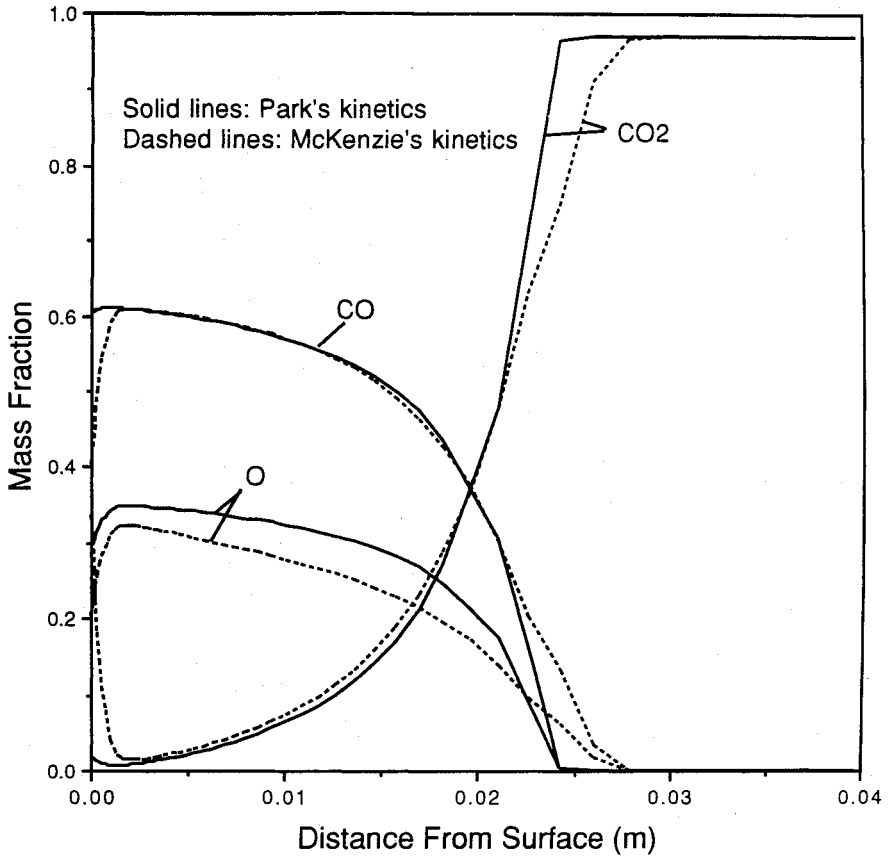

Fig. 3b Mass fractions along stagnation streamline.

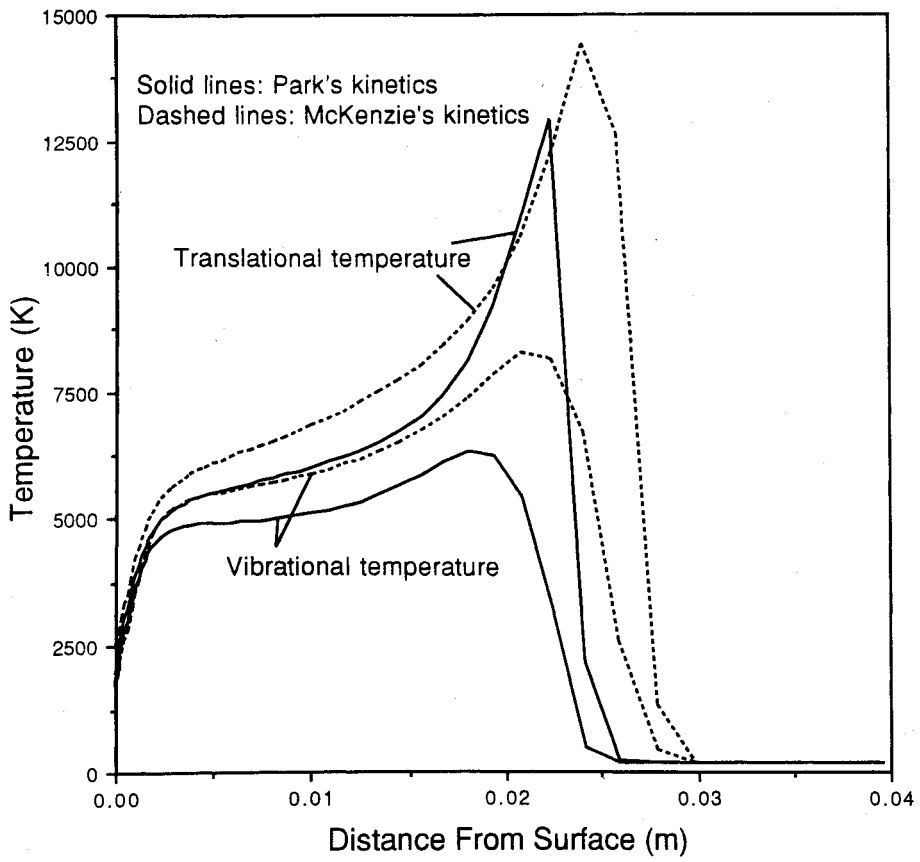

Fig. 3c Temperature profiles along stagnation streamline.

MESUR probe. Figure 2 presents the resulting normalized surface heating to a 70-deg half-angle sphere cone predicted by the Navier-Stokes code and is compared with data taken from the NASA Ames 1.07-m (42-in.) shock tunnel experiment. For the shock tunnel test case, $H_t = 4.7$ MJ/kg, $P_t = 0.0516$ atm, $R_c/R_n = 0.1152$, $R_b/R_n = 1.94$, and $R_n = 0.038$ m. The freestream species concentrations in the Navier-Stokes calculation are estimated based on a nozzle exit $M_f = 3.5$. The model surface for this test case is assumed to be cold, isothermal ($T_w = 360$ K), and fully catalytic. Park's gas kinetic model is applied. Because of many uncertainties in the freestream conditions, flow properties, and surface conditions, the surface heating rates presented in Fig. 2 are normalized relative to their stagnation point value. Generally speaking, the predicted heat-flux distribution agrees with the shock tunnel data, and this comparison suggests that the computations are internally consistent.

Using the peak heating trajectory point conditions for the MESUR probe during Mars atmospheric entry, several complete solutions were obtained for a variety of gas kinetics, surface catalysis, diffusion coefficients, and thermal conductivities. The freestream conditions are listed in Table 2. The Reynolds number $R_e = 1.2 \times 10^4$ (based on R_n) is high enough to insure that the assumptions of continuum flow and no slip at the surface are valid. The uncertainty on the grid resolution has been carefully monitored so as not to affect any conclusion drawn later in this study.

The effect of gas kinetics on the surface radiative equilibrium temperature distribution of a noncatalytic wall is shown in Fig. 3a. Species concentrations and flow temperatures along the stagnation streamline are shown in Figs. 3b and 3c. The surface temperature predicted from McKenzie's gas kinetics (dashed line) is higher than that from those of Park (solid line). Near the stagnation point, the surface temperature using McKenzie's gas kinetics is about 100 K higher than that based on Park's kinetics. The difference in the surface temperature decreases slightly as the distance from the stagnation point increases, and the high temperature region around the shoulder for McKenzie's kinetics appears to be relatively weak compared with Park's. The temperatures (both vibrational and translational) along the stagnation streamline for McKenzie's kinetics are significantly higher than those for Park's kinetics, and thus the shock standoff distances are different between two models. This difference is related to the fact that the local specific heat ratio depends on composition that changes with different chemical reaction rates.

Figure 4 shows CO_2 forward reaction rates for both gas kinetics models used in this study. Both models give about the same rates at temperatures near 5000 K. At higher temperatures, Park's kinetics predict faster rates, but the difference between the two models is less than an order of magnitude. However, at low temperatures, McKenzie's model predicts reaction rates about five orders of magnitude higher than Park's model. The species concentration profiles shown in Fig. 3b reflect these differences. In the high-temperature region (near the shock), the solutions for Park's kinetics predict slightly higher gradients of species concentrations, and in the low-temperature region (near the surface), McKenzie's kinetics predict an extremely sharp change in the CO_2 and CO concentrations.

The effects of surface catalysis on the heating rates to the wall are presented in Figs. 5 and 6. The predictions shown in Fig. 5 are calculated using the current Navier-Stokes code, and those in Fig. 6 are calculated from the viscous shock layer (VSL) code of Chen[7] (adapted from the original code of Gupta

Table 2 Freestream conditions for MESUR

Altitude, m	Velocity, m/s	Density, kg/m^3	Temperature, K	C_{CO_2}	C_{N_2}
41,668	6155	0.2687×10^{-3}	160.9	0.9685	0.0315

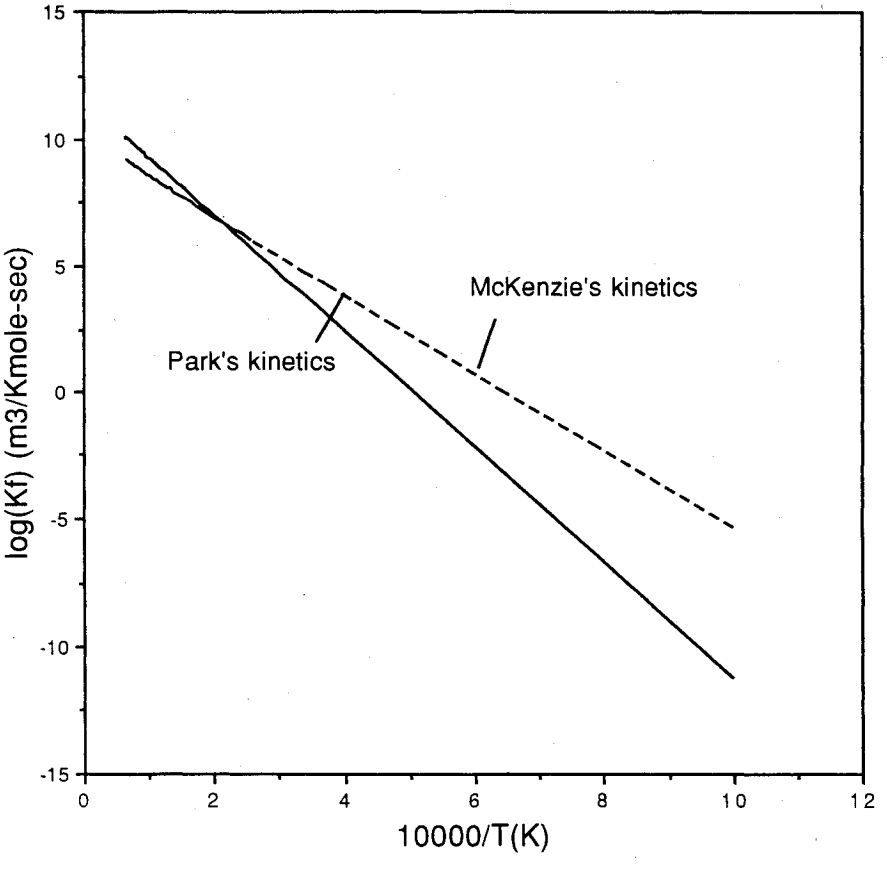

Fig. 4 Forward reaction rates ($CO_2 + M \rightarrow CO + O + M$).

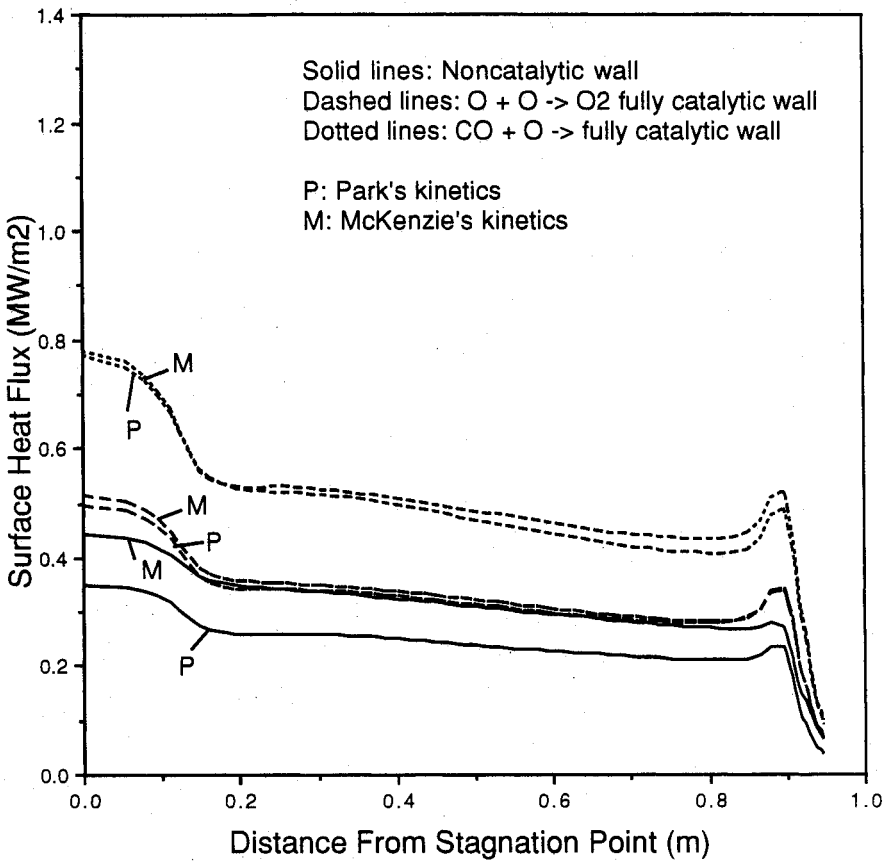

Fig. 5 Effect of surface catalysis on surface heating (Navier-Stokes solutions).

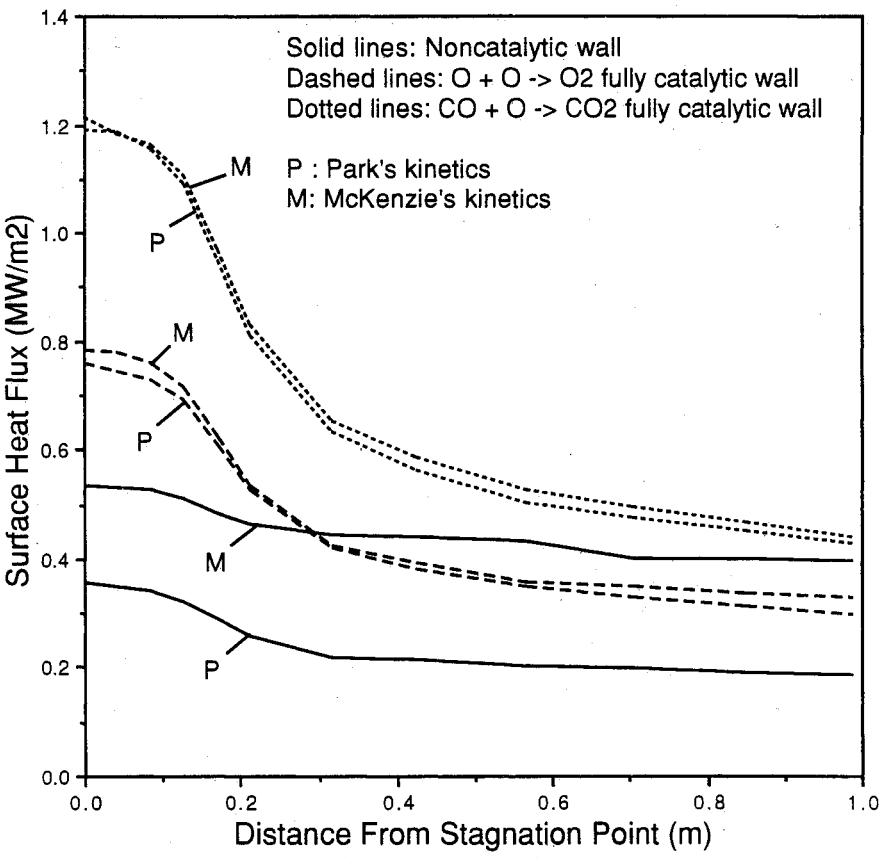

Fig. 6 Effect of surface catalysis on surface heating (VSL solutions[7]).

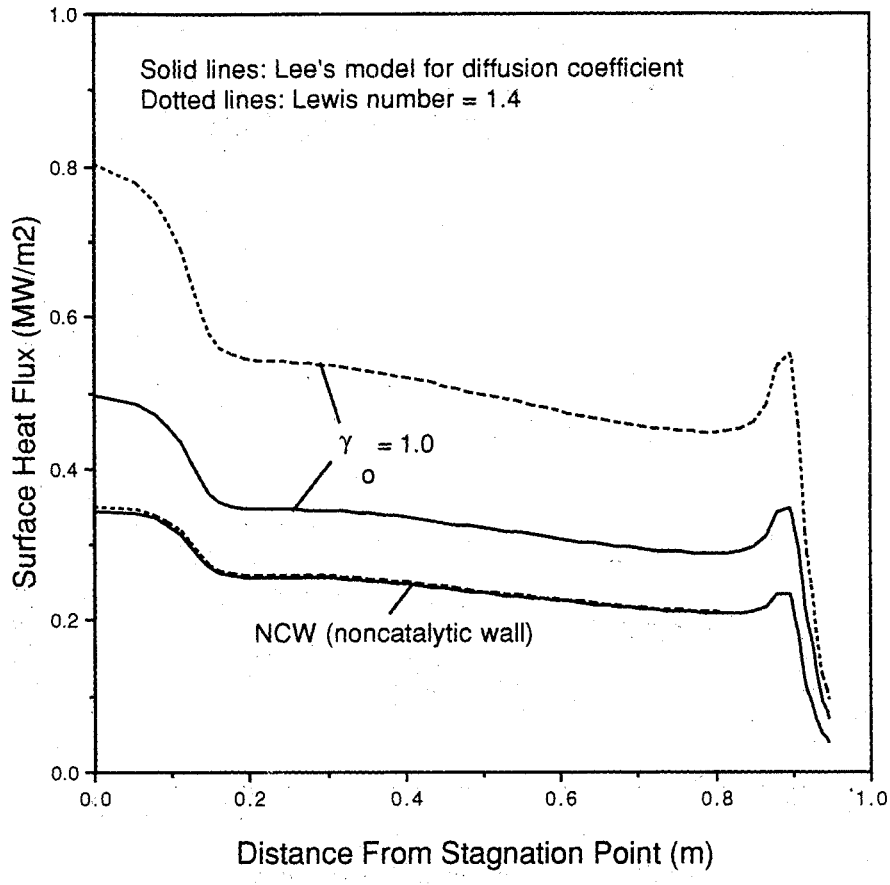

Fig. 7a Effect of diffusion coefficient on surface heating.

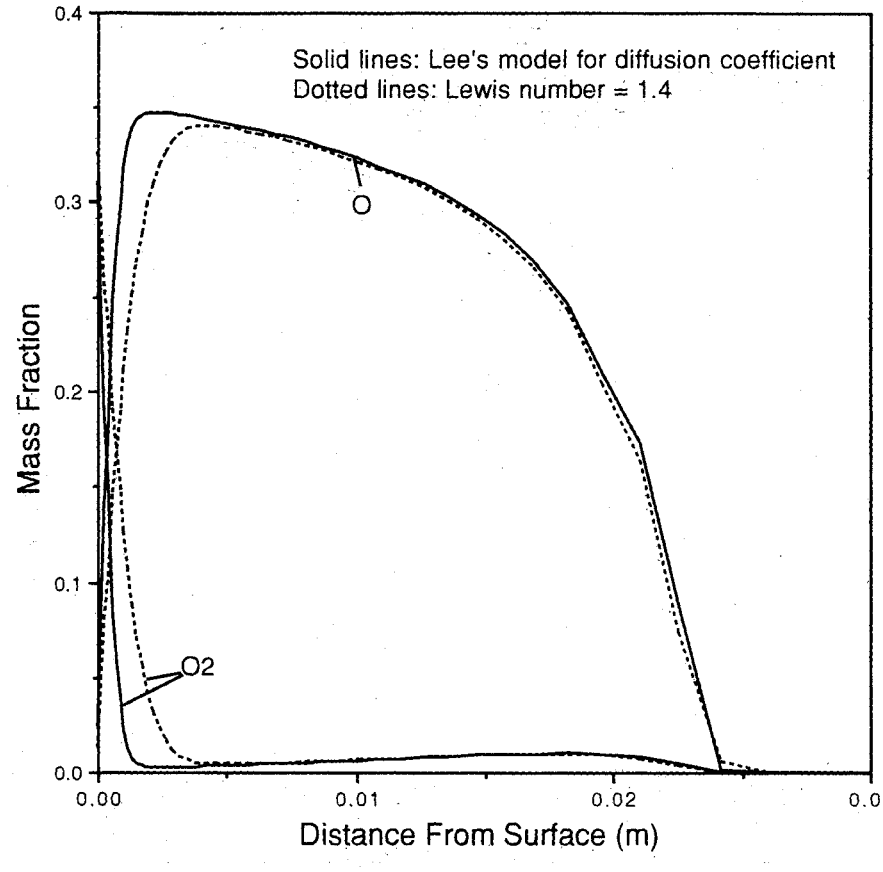

Fig. 7b Effect of diffusion coefficient on species concentration along stagnation streamline.

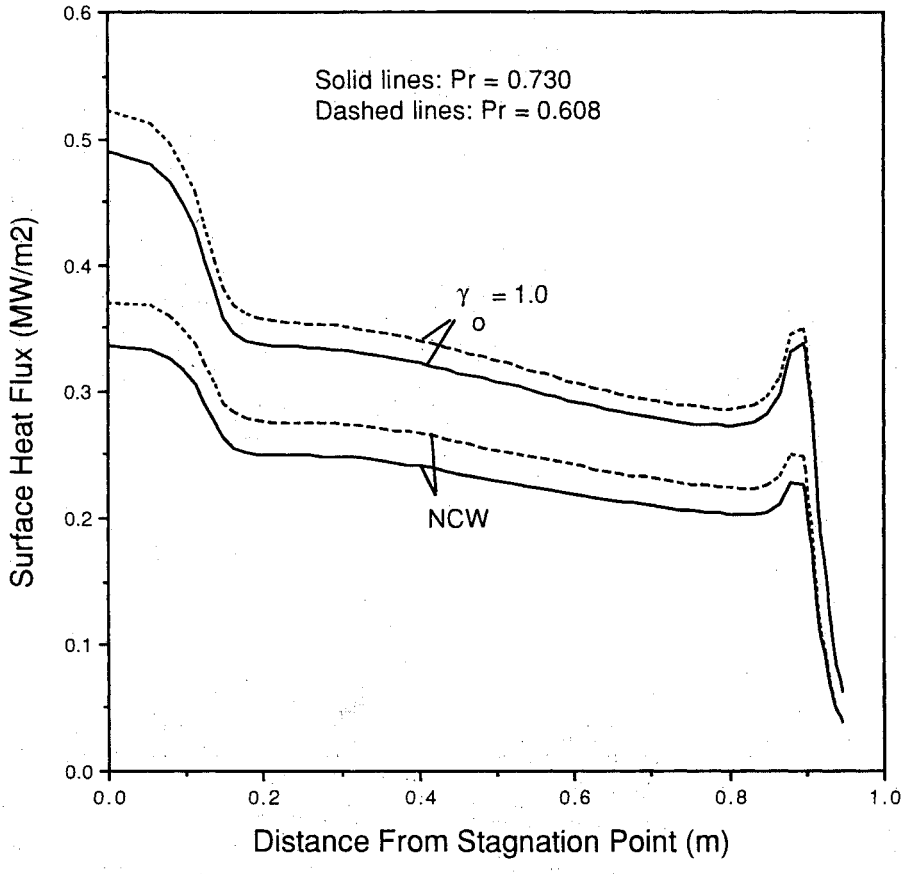

Fig. 8 Effect of thermal conductivity on surface heating.

and Simmonds[10]). The results for the noncatalytic wall (solid lines), the fully catalytic wall with only $O + O \rightarrow O_2$ (dashed lines), and the fully catalytic wall with only $CO + O \rightarrow CO_2$ (dotted lines) with two sets of gas kinetics are presented.

The Navier-Stokes solutions in Fig. 5 show that the heat flux to the noncatalytic wall that is predicted with Park's gas kinetics is about 80% of that predicted with McKenzie's model. Also, the surface heating to the fully catalytic wall appears to be relatively insensitive to the gas kinetic models because all of the available recombination energy is released. The stagnation point heating for the CO_2 fully catalytic wall is about 2.2 times that for the noncatalytic wall with Park's gas kinetics, and that for the O_2 fully catalytic wall is about 1.4 times. McKenzie's kinetic rate data were originally developed based on the translational temperature. However, the effect of thermal nonequilibrium (two-temperature model) on the surface heating and global flow structure is negligibly small for the case we examined here,[24] and, as mentioned earlier, the major difference between both kinetic rate data is in the low-temperature region, in which the flow is in near or full thermal equilibrium (Fig. 3c). Thus, employing a geometric average temperature in McKenzie's kinetics model in the Navier-Stokes calculations has little effect on the accuracy of these solutions.

As a comparison with the present Navier-Stokes (N-S) calculations, and to show the importance of accounting for the extreme bluntness and corner effects of the flight body, computations are presented for the MESUR probe using the VSL code[7] mentioned earlier. The VSL code uses a one-temperature model. Hence, all of the gas reaction rates were calculated based on translational temperature. The viscous shock layer equations solved here use a finite difference, space-marching, shock-fitting method developed by Davis.[25] (The details of these VSL calculations and solutions were discussed previously by Chen[7].) The transport and thermodynamic properties implemented in this VSL code are different from those in the Navier-Stokes code. The VSL code is not able to solve for the flow over a sphere cone of finite length, and therefore the VSL solutions presented here are for an infinitely blunted cone. Thus, the corner effect does not appear in these solutions. Generally speaking, the distributions predicted by the two codes are different, and the VSL code predicts higher surface heating than does the N-S code. This is particularly true for the fully catalytic wall. For the noncatalytic wall with Park's kinetics, the stagnation point heat transfer rates predicted by the two codes are in good agreement; the VSL solution is only slightly higher. Surface heating over the forebody heatshield is sensitive to many parameters, such as transport and thermodynamic properties and gas kinetics, as well as the position of the bow shock wave in front of the vehicle. The VSL solution predicted a smaller bow shock wave standoff distance (7% smaller) and used a diffusion coefficient five times higher than those in the Navier-Stokes solutions. Because of the many different features within the two codes, the influence of these parameters on the comparison of predicted surface heating distributions is not clear at this time.

Because of these uncertainties, a systematic study of the effect of the transport properties on surface heating was performed using the present Navier-Stokes code. First, the effect of diffusion coefficient differences on the surface heating rate distribution is examined by comparing results using Lee's diffusion model with those using a Lewis number equal to 1.4 (Fig. 7a). The solid lines are the predictions for Lee's model,[11] and the dotted lines are those for L_e equal to 1.4. The constant L_e number model is usually considered to be a reasonable assumption in many engineering applications and is used in the VSL code. When comparing the diffusion coefficients calculated from these two models, those predicted with $L_e = 1.4$ are about five times as high as those with Lee's model in the region near the surface where diffusion processes are important relative to convective processes. For a noncatalytic wall, the effect of diffusion coefficients on the surface heating

is negligible. However, for the fully catalytic wall (where $O + O \rightarrow O_2$), the heat flux prediction for the case with $L_e = 1.4$ is about 60% higher than that for Lee's model. As shown in Eq. (22), thermal conduction is the main contributor to surface heating, since the species concentration gradients are zero for a noncatalytic wall. Therefore, the contribution of mass diffusion to surface heating will become significant when the surface catalytic effect is important.

A comparison of species concentrations along the stagnation streamline between two mass diffusion models is shown in Fig. 7b. The two models have a large effect on the species concentration profiles only within the boundary layer and do not affect the shock standoff distance. A thicker boundary layer results from the solution for $L_e = 1.4$ because of the larger diffusion coefficients. Even without a correct mass diffusion model, for high Reynolds number flow the Navier-Stokes code is still able to resolve most of the flow structure, including shock standoff distance, since the diffusion processes are confined to a very small region near the surface. Therefore predicted flows that have exactly the same shock standoff distance may have dramatically different surface heating rates. Global flow structure is relatively insensitive to the uncertainty in the transport properties; however, the transport properties become very critical for the near surface flow structure and associated surface heating distributions.

The effect of thermal conductivity on the surface heating is presented in Fig. 8. Solid lines show the solutions for $P_r = 0.73$, and the dashed lines show the solutions for $P_r = 0.608$ (thermal conductivity increased by 20%); $P_r = 0.73$ has been used in many air flow calculations. The solutions indicate both catalytic and noncatalytic walls are affected by the variation in thermal conductivity. The effect on the heat flux to the noncatalytic wall appears to be slightly higher than to the fully catalytic wall. The effect in the stagnation point region is more significant than over the downstream region of the forebody.

Conclusions

Two-dimensional axisymmetric Navier-Stokes solutions with a two temperature and multispecies transport-reaction model have been obtained for the direct Mars atmospheric entry of a small probe. These solutions include the boundary conditions to account for surface energy balance and catalysis. The results indicate surface catalysis effects for the CO_2-N_2 system will highly increase the heat-transfer rate to the surface. Thus, to accurately predict surface heating in these cases, knowledge of surface kinetics is essential. For a noncatalytic wall, the surface heating is sensitive to gas kinetics. Heating rates predicted with Park's kinetics are lower than the predictions with McKenzie's kinetics. However, for a fully catalytic wall, the surface heating is relatively insensitive to the gas kinetic models. The predictions also show that the surface heating rates are sensitive to the models used for transport properties (thermal conductivity and mass diffusivity), especially for highly catalytic walls.

This study shows that the accurate prediction of surface heating rate is more difficult than predicting global flow structure. The prediction of surface heating over a large-angle blunted body in a thermochemically nonequilibrium flow requires a robust computational fluid dynamics code to solve the Navier-Stokes equations with appropriate physics and chemistry and an optimized mesh to resolve the shock structure as well as the flow-surface interactions. Regardless of the uncertainties due to the numerical technique and grid procedures, the accuracy of the calculation depends on the accuracy of the physical and chemical models implemented into the code. The uncertainties of current available models for gas kinetics, transport properties, and vibrational relaxation in a CO_2-N_2 mixture should be thoroughly examined. It is, therefore, urgent to proceed with the development of a surface kinetic model for CO_2-N_2 mixtures. Once this is done, it will be possible to meaningfully assess the accuracy of surface heating calculations for future NASA Mars entry missions.

References

[1]Evans, J. S., Schexnayder, C. J., Jr., and Grose, W. L., "Effects of Nonequilibrium Ablation Chemistry on Viking Radio Blackout," *Journal of Spacecraft and Rockets,* Vol. 11, No. 2, 1974, pp. 84–88.

[2]Candler, G. V., "Computation of Thermo-Chemical Non-equilibrium Martian Atmospheric Entry Flows," AIAA Paper 90-1695, Jan. 1990.

[3]McKenzie, R. L., "An Estimate of the Chemical Kinetics Behind Normal Shock Waves in Mixtures of Carbon Dioxide and Nitrogen for Conditions Typical of Mars Entry," NASA TN D-3287, Jan. 1966.

[4]Park, C., Howe, J. T., Jaffe, R. L., and Candler, G. V., "Chemical-Kinetic Problems of Future NASA Missions," AIAA Paper 91-0464, Jan. 1991.

[5]Stewart, D. A., Rakich, J. V., and Lanfranco, M. J., "Catalysis Surface Effects on Space Shuttle Thermal Protection System During Earth Entry of Flights STS-2 Through STS-5," NASA CP2283, March 1983.

[6]Stewart, D. A., Chen, Y.-K., and Henline, W. D., "Effect of Non-Equilibrium Flow Chemistry and Surface Catalysis on Surface Heating to AFE," AIAA Paper 91-1373, June 1991.

[7]Chen, Y.-K., "Effect of Nonequilibrium Flow Chemistry on the Heating Distribution over the MESUR Forebody During a Martian Entry," NASA Contract Rept., NAS2-13210, June 1991.

[8]Inouye, M., Rakich, J. V., and Lomax, H., "A Description of Numerical Methods and Computer Programs for Two-Dimensional and Axisymmetric Supersonic Flow Over Blunt-Nosed and Flatted Bodies," NASA TN D-2970, May 1965.

[9]Bartlett, E. P., and Kendall, R. M., "An Analysis of the Coupled Chemically Reacting Boundary Layer and Charring Ablator, Part III: Nonsimilar Solution of the Multicomponent Laminar Boundary Layer by an Integral Matrix Method," NASA CR-1062, June 1968.

[10]Gupta, R. N., and Simmonds, A. L., "Stagnation Flowfield Analysis for Aeroassist Flight Experiment Vehicle," AIAA Paper 88-2613, June 1988.

[11]Lee, J. H., "Basic Governing Equations for the Flight Regimes of Aeroassisted Orbital Transfer Vehicles," *Thermal Design of Aeroassisted Orbital Transfer Vehicles,* edited by H. F. Nelson, Vol. 96, Progress in Astronautics and Aeronautics, AIAA, New York, 1985, pp. 3–53.

[12]Tauber, M. E., and Sutton, K., "Stagnation-Point Radiative Heating Relations for Earth and Mars Entries," *Journal of Spacecraft and Rockets,* Vol. 28, No. 1, 1991, pp. 40–42.

[13]Vincenti, W. G., and Kruger, C. H., Jr., *Introduction to Physical Gas Dynamics,* Krieger, Malabar, FL, July 1965.

[14]Millikan, R. C., and White, D. R., "Systematic of Vibrational Relaxation," *Journal of Chemical Physics,* Vol. 39, No. 12, 1963, pp. 3209–3213.

[15]Park, C., "Assessment of Two-Temperature Kinetic Model for Ionizing Air," AIAA Paper 87-1574, Jan. 1987.

[16]Kolodziej, P. K., and Stewart, D. A., "Nitrogen Recombination on High Temperature Reusable Surface Insulation and the Analysis of Its Effect on Surface Catalysis," AIAA Paper 87-1637, June 1987.

[17]Wilke, C. R., "A Viscosity Equation for Gas Mixtures," *Journal of Chemical Physics,* Vol. 18, No. 4, 1950, p. 517.

[18]Blottner, F. G., Johnson, M., and Ellis, M., "Chemically Reacting Viscous Flow Program for Multi-Component Gas Mixtures," Sandia National Labs., SR-RR-70-754, Albuquerque, NM, Feb. 1971.

[19]Candler, G. V., "The Computation of Hypersonic Ionized Flows in Chemical and Thermal Nonequilibrium," AIAA Paper 88-0511, Jan. 1988.

[20]MacCormack, R. W., "Current Status of Numerical Solutions of the Navier-Stokes Equation," AIAA Paper 85-0032, Jan. 1985.

[21]Candler, G. V., and MacCormack, R. W., "Hypersonic Flow Past 3-D Configurations," AIAA Paper 87-0480, June 1987.

[22]Tam, L. T., and Li, C. P., "Comparison of Thermochemical Nonequilibrium Viscous Flowfield Predictions for AFE Vehicle," AIAA Paper 91-1371, June 1991.

[23]Gnoffo, P. A., Price, J. M., and Braun, R. D., "On the Computation of Near Wake Aerobrake Flow Fields," AIAA Paper 91-1371, June 1991.

[24]Chen, Y.-K., Henline, W. D., Stewart, D. A., and Candler, G. V., "Navier-Stokes Solutions with Surface Catalysis for Martian Atmospheric Entry," AIAA Paper 92-2946, July 1992.

[25]Davis, R. T., "Numerical Solution of the Hypersonic Viscous Shock-Layer Equations," *AIAA Journal,* Vol. 8, No. 6, 1970, pp. 834–851.

Michael E. Tauber
Associate Editor